Biosensors and Bioelectronics 143 (2019) 111596

Contents lists available at ScienceDirect

Biosensors and Bioelectronics

journal homepage: www.elsevier.com/locate/bios

Plasmonic-3D photonic crystals microchip for surface enhanced Raman spectroscopy

Guojian Chen[a], Kelian Zhang[a], Baibin Luo[b], Wei Hong[a,*], Jian Chen[b], Xudong Chen[a,**]

[a] Key Laboratory for Polymeric Composite and Functional Materials of Ministry of Education, School of Chemistry, Sun Yat-sen University, Guangzhou, 510275, China
[b] Instrumental Analysis and Research Center, Sun Yat-sen University, Guangzhou, 510275, China

ARTICLE INFO

Keywords:
Three dimensional photonic crystals
Plasmonic particles
Surface enhanced-Raman scattering
Slow-photon effect
Microchips
Biosensor

ABSTRACT

Plasmonic-dielectric hybrid substrates of Ag-islands on three-dimensional photonic crystals are fabricated through magnetron sputtering of silver onto hydrophobized silica photonic crystals, free from etching process. Without typical "hot-spots" such as nanogaps, significant Raman enhancements can be achieved, attributed to the enhanced electromagnetic field and scattering of the plasmonic nanoparticles as well as the enhanced light-matter interaction by the slow photon effects. The detection limit for adenine by the hybrid substrates reaches nM level, with a calculated enhancement factor of 1.13×10^7, which is three orders of magnitude higher than the conventional noble metal film over nanosphere (FON) control group. Furthermore, microchips based on the hybrid substrates are facilely achieved, enabling micro-detection through super hydrophobic concentration. The facile fabrication and effective Raman enhancements make the Ag-islands on 3D photonic crystals promising candidates in the field of chemical sensors, Raman mapping and bioassays.

1. Introduction

Surface enhanced Raman spectroscopy (SERS) has overcome the major drawbacks of normal Raman spectroscopy, its weak signal intensity and low sensitivity (Kneipp et al., 2006; Ding et al., 2016). Owing to its ultrahigh sensitivity and specificity, the potential of SERS has been greatly exploited in extensive domains, such as single-molecule detection (Nie and Emory, 1997), chemical analysis (Sharma et al., 2012), medical diagnoses (Chen et al., 2016), sensing for pollutants (Li et al., 2010; Zhao et al., 2015a), explosives (Gong et al., 2014), and pesticides (Yang et al., 2014).

It has gained wide acceptance that the SERS effect can be attributed to the electromagnetic factor (Prodan et al., 2003; Gruenke et al., 2016), as well as the chemical factor (Campion and Kambhampati, 1998; Liu et al., 2016). The former can elucidate the dramatic enhancement and distance dependence of SERS (Schatz et al., 2006; Schlücker, 2014), and the latter can explain its selectivity to detect molecules (Campion and Kambhampati, 1998). The enhancement of Raman scattering is proportional to the fourth power of the enhancement of local electric field, which is usually induced by the localized surface plasmon resonances (LSPR) of metal nanostructures (Schlücker, 2014; Ding et al., 2016). Great effort has been made to achieve high Raman enhancement factor (EF) by highly localized regions ("hot spots") of the junctions between two plasmonic particles (Zhu et al., 2016; Nam et al., 2016). The "hot spots" strategy is effective for the plasmonic SERS substrates of metal colloids and nanostructured arrays, achieving 10^{14} increase in the molecular Raman scattering cross-section for trace detections or even single-molecule levels (Nie and Emory, 1997; Wang et al., 2013).

Periodically dielectric materials has been a powerful nanofabrication approach to achieve regular hybrid SERS substrates with the plasmonic nanostructure (Banholzer et al., 2008; Schlücker, 2014). Such submicroscale periodically structures for SERS are mainly comprised of three types: noble metal film over nanosphere (FON) structures (Zhang et al., 2005; Fang et al., 2008), SERS-active photonic crystal fibers (Kang et al., 2009; Gong et al., 2015), and three dimensional photonic crystals (Qi et al., 2014; Zhao et al., 2015b). The FON technique refers to a templating method based on a monolayer of close-packed nanospheres, which is tunable to regulate the LSPR property of the hybrid strucutre (Zhang et al., 2005; Fang et al., 2008; Hong et al., 2015). Typical FON substrates can cause EF at 10^3-10^6 (Baia et al., 2006; Flores-Romero et al., 2018). With "hot spots" introduced into the hybrid structure, the EF of the FON structure could reach over 10^{14}, due to the strong field intensity at the nanogaps (Im et al., 2013; Zhang et al., 2017). The SERS-active photonic crystal fibers are based on the oscillators in the middle of the fibers, which can lead to a much longer

* Corresponding author.
** Corresponding author.
E-mail addresses: hongwei9@mail.sysu.edu.cn (W. Hong), cescxd@mail.sysu.edu.cn (X. Chen).

https://doi.org/10.1016/j.bios.2019.111596
Received 11 June 2019; Received in revised form 11 August 2019; Accepted 13 August 2019
Available online 14 August 2019

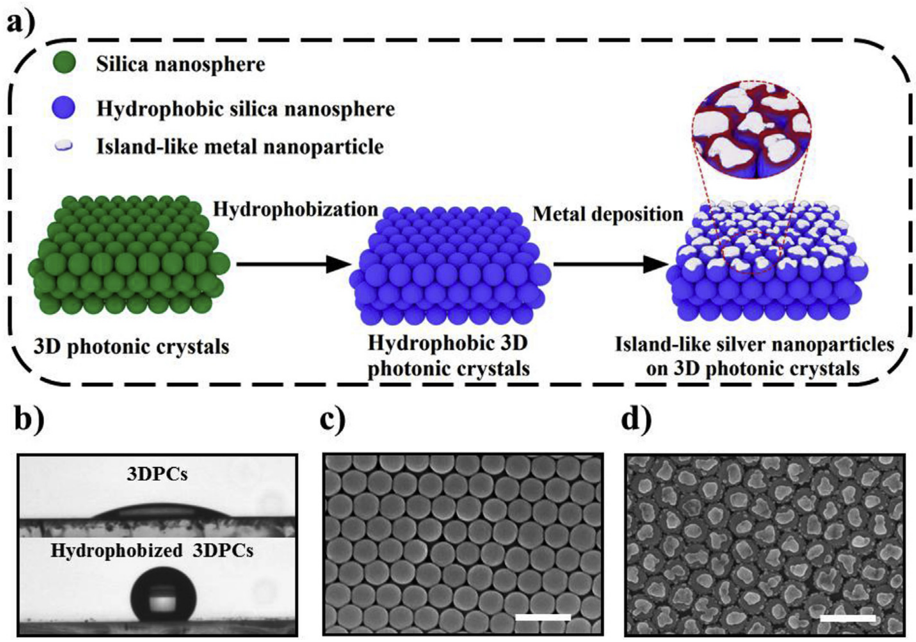

Fig. 1. (a) Schematic showing the fabrication procedure of 3D-islands hybrid substrates from 3D photonic crystals. (b) Contact angles of 3DPCs before and after the hydrophobization. The SEM images of (c) hydrophobized 3DPCs and (d) 3D-islands. The diameters of SiO_2 spheres were 242 nm (stop band at 526 nm). Scale bar: 500 nm.

light interaction length by the multiple reflection (Kang et al., 2009; Gong et al., 2015). The three dimensional periodically dielectric materials, such as inverse opal structures, lead to enhanced matter-light interaction by the slow photon effects (Qi et al., 2014; Sun et al., 2016, 2017) as well as the enhanced adsorption of analytes by the interconnected channels (Qi et al., 2014; Zhao et al., 2015b), which can benefit the SERS detection. Despite these reports on the plasmonic-photonic crystals hybrid structure for SERS substrates, scalable and reproducible structures with high sensitivity and low noble metals consumption are still challenging. In addition, high energy exposure and complex etching process for achieving hot spots on FONs restricted their practical applications.

In this work, we demonstrate a plasmonic-3D photonic crystals hybrid SERS substrate with significant SERS enhancement through sputtering deposition of silver on chemically hydrophobized three-dimensional photonic crystals without any etching process. The hybrid SERS substrates (denoted as 3D-islands) consist of Ag-islands on three-dimensional photonic crystals (3DPCs). Great Raman enhancement could be achieved due to the enhanced scattering between the metal nanoparticles and the 3DPCs as demonstrated by the reflectance spectra. In addition, the slow photon effects by the photonic band edge and the enhanced electromagnetic field by the hybrid structure are demonstrated to contribute to the SERS. The enhancement factor of the 3D-islands show three orders of magnitude higher than the conventional noble metal film over nanosphere (FON) control group. The hybrid substrate also demonstrated competitive detection ability in simulated biological environment. Furthermore, microchips based on the hybrid substrates are constructed, enabling micro-detection and further reducing the detection limit through super hydrophobic concentration. This study provides a convenient method for the manufacture of hybrid substrates without complex etching process, which is cost-efficient, reproducible with spatially uniform and high enhanced factor, showing tremendous potential for the biological and chemical detection.

2. Experiments

2.1. Synthesis of monodispersed SiO_2 spheres

Monodispersed SiO_2 spheres, with diameters ranging from 198 to 313 nm, were synthesized through improved Stöber method (see the supplementary material) (Stöber et al., 1968; Sun et al., 2016).

2.2. Preparation of SiO_2 3D photonic crystals films

SiO_2 3D photonic crystals films were prepared through improved vertical deposition method (see the supplementary material).

2.3. Preparation of SiO_2 2D photonic crystals for comparison

SiO_2 2D photonic crystals films were self-assembled at the air/water interface. Details was showed in the supplementary material.

2.4. Hydrophobization of SiO_2 photonic crystals

Through 2 h of chemical vapor deposition, the obtained SiO_2 photonic crystals were modified with 1H,1H,2H,2H-perfluorodecyltrichlorosilane (50 mL) in a desiccator.

2.5. Fabrication of hybrid substrates

Using KYKY SBC-12 compact ion sputter coater, silver was deposited onto the substrates (see the supplementary material).

2.6. Immobilization of adenine and methylene blue

For the immobilization of adenine, substrates were immersed in 40 mL of adenine aqueous solution with different concentrations for 1 h, followed by rinse with pure water. For methylene blue (MB) immobilization, 20 μL of MB aqueous solutions with different concentrations were drop-casted on the substrates. All of the substrates were dried in air at 40 °C before SERS analysis.

3. Results and discussion

3.1. Morphology and optical properties

The procedure for the preparation of the 3D-islands sample is illustrated in Fig. 1a. Briefly, silver was deposited onto the hydrophobic SiO_2 3DPCs. And due to the low surface tension of hydrophobic 3DPCs (Fig. 1b), the deposited silver tended to split into island-like structure on top of the SiO_2 spheres (Fig. 1d). The hydrophobic 3DPCs kept the solution and analyte on the surface where island-like silver particles existed (Fig. S1).

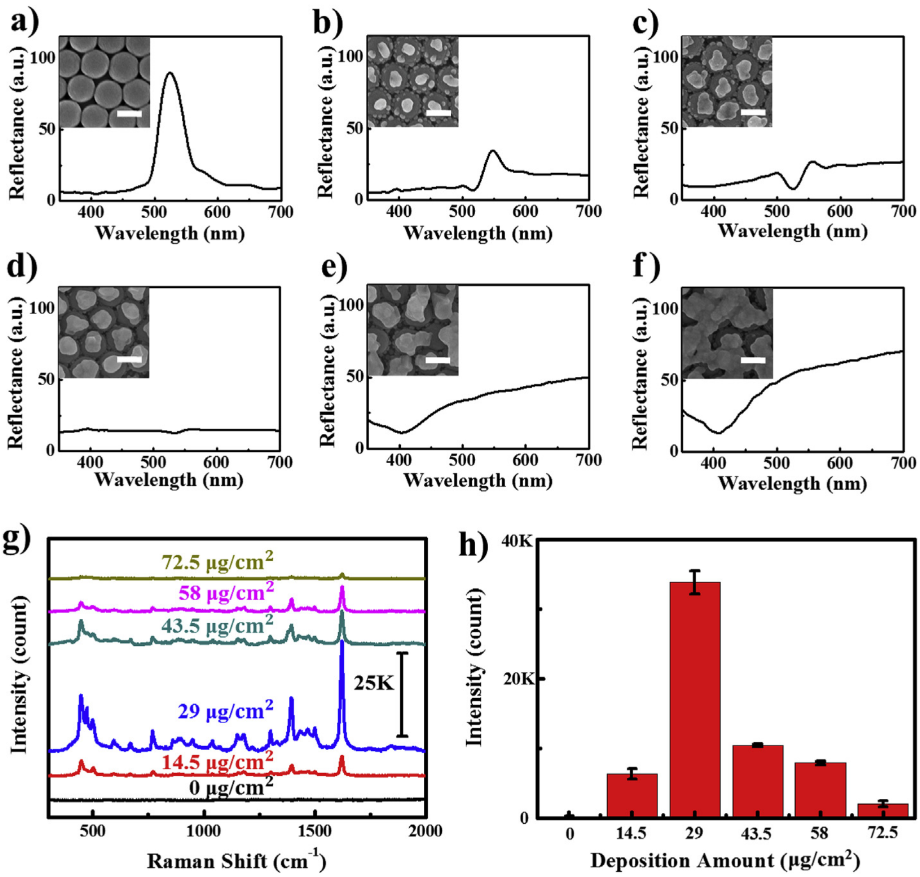

Fig. 2. Normal-incident reflectance spectra of hybrid substrates with different silver deposition amountof (a) 0, (b) 14.5 μg/cm^2, (c) 29 μg/cm^2, (d) 43.5 μg/cm^2, (e) 58 μg/cm^2 and (f) 72.5 μg/cm^2 on hydrophobic 3DPCs, respectively. The diameters of SiO_2 spheres were 242 nm (stop band at 526 nm). Inset: the corresponding SEM images of the samples, scale bar: 200 nm. The complete images of the insets were provided in Fig. S2. (g) Raman spectra of 10^{-6} M MB applied on substrates with various silver deposition amount and (h) their Raman intensity at 1625 cm^{-1} versus sputtering amount. The excitation wavelength was 633 nm. The intensity represented the average value from five SERS spectra. The diameters of SiO_2 spheres were 242 nm (stop band at 526 nm).

The silver structures showed significant impacts on the reflectance spectra of the 3DPCs (Fig. 2). Compared with the reflactance feature of 3DPCs (Fig. 2a), the reflactance reduced as the deposited silver increased from 14.5 μg/cm^2 to 43.5 μg/cm^2 (Fig. 2b–d). When the deposited silver increased from 14.5 μg/cm^2 to 29 μg/cm^2, the diameters of the plasmonic particles increased from 90 nm to 150 nm. Accordingly, the photonic stop band of the 3DPCs (Fig. 2a) showed dip within the photonic stop band (Fig. 2b and c), which was caused by the multiple scattering between the plasmonic nanoparticles and the Bragg reflector (Lin et al., 2015; Chen et al., 2017). Further silver deposition led to the disappearance of the dip feature in the reflectance spectra, where the scattering and reflectance of the silver layer dominated the reflectance properties of the films, as very limited light could transmit through the silver layer (Fig. 2d–f). The complete images of the insets were provided in Fig. S2.

The SERS activity highly depended on the morphology and optical properties of the hybrid substrates. To evaluate the SERS performance of 3D-islands, SERS spectra were measured on the samples functionazed with methylene blue (MB) through drop-casting. As shown in Fig. 2g, the most distinct peaks at 1397 cm^{-1} and 1625 cm^{-1} in the acquired Raman spectrawere assigned to C–H in-plane ring deformation and C–C ring stretching mode respectively (Guo et al., 2012), and the peaks at 448 cm^{-1} and 499 cm^{-1} were arising from C–N–C skeletal bending mode (Xiao and Man, 2007). The hydrophobic 3DPCs showed no distinguishable Raman peak of MB, indicating the limited enhancement by the 3DPCs. The size distribution of silver islands on 3DPCs was shown in Fig. S3 to Fig. S7. The maximal Raman enhancement was observed for 3D-islands with silver thickness of 29 μg/cm^2. With such silver deposition amount, 70.37% of the silver islands with size distributed between 15,000 nm^2 and 20,000 nm^2 (Fig. S4). And it was considered that the optimal size of silver islands was between 15,000 nm^2 and 20,000 nm^2. Moreover, the 3D-islands with silver thickness of 29 μg/cm^2 exhibited the most significant reflectance dip (Fig. 2c) as a result of the most effective multiple scattering between the plasmonic Ag-islands and the 3DPCs Bragg reflector (Lin et al., 2015; Chen et al., 2017), indicating that the system had enough transmitance through the silver layer to maximize the scattering and light-matter interactions enhanced by photonic stop bands. As the oversize silver particles limited the transmitance through the silver layer to 3DPCs and reduced scattering, while the undersize silver islands could only receive limited reflected light from the 3DPCs. In both cases, the multiple scattering between the plasmonic silver islands and the 3DPCs Bragg reflector could not be fully utilized. Only with appropriate size of silver islands on the 3DPCs, the hybrid substrate could realize greatest Raman enhancement (Fig. 2h).

The SERS activity of the 3D-islands could be ascribed to the enhanced scattering and electromagnetic field as demonstrated by the finite-difference time-domain (FDTD) stimulation, using the model in Fig. S8. According to the $|E|^2$ on the surface when excited by incident light at 633 nm (Fig. S9 and Fig. S10), the samples with silver particle diameter between 125 nm and 150 nm exhibited the maximal $|E|^2$, in accordance with the experimental fact that the 3D-islands with silver thickness of 29 μg/cm^2 (silver particle size of 150 nm) showed the highest Raman enhancement.

3.2. *Slow photon effects on SERS*

In order to investigate how photonic stop bands impacted on the Raman enhancement, a series of 3D-islands samples were prepared with diverse stop bands ranging from 431 nm to 695 nm (Fig. S11 and Fig. S12). Subsequently, the 3D-islands samples were functionalized with adenine by adsorption in 5×10^{-7} M solution, followed by Raman measurements. After the reflectance characteristics of 3D-islands were confirmed to remain unchanged after the adenine adsorption (Fig. S13), the Raman enhancement was evaluated by the intensity of the dominant peak at 734 cm^{-1}, which was assigned to the ring breathing mode

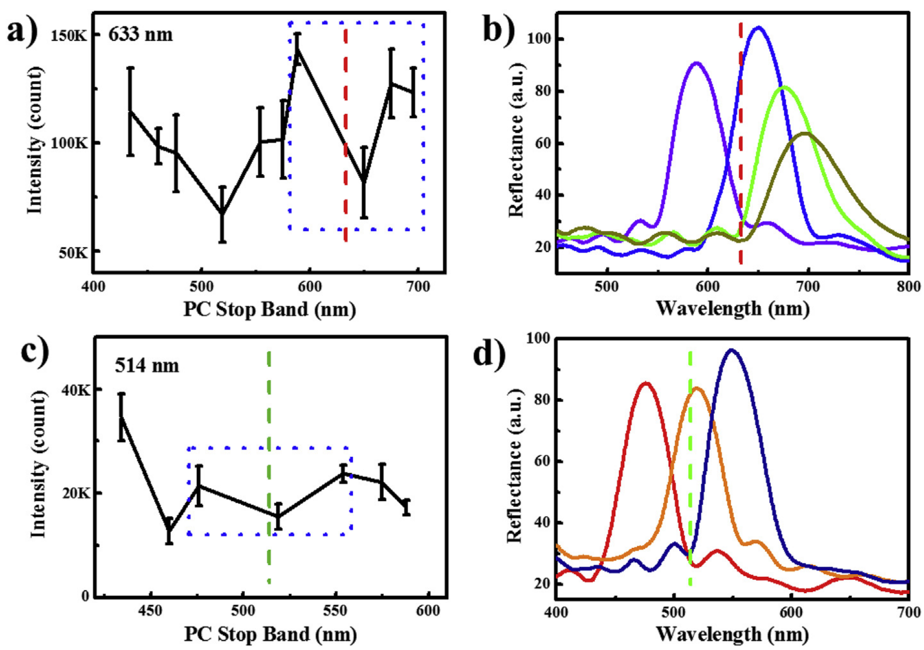

Fig. 3. Raman intensity at 734 cm^{-1} on the 3D-islands with different stop bands, (a) excited by 633 nm and (c) 514 nm laser, respectively. The dash lines indicated the excitation wavelengths and the dots rectangles indicated the region where stop bands interacted with the excitation wavelengths. (b) and (d) The stop bands and excitation wavelengths corresponded to the dots rectangles in (a) and (c), respectively. All 3D-islands substrates were of 29 $\mu g/cm^2$ silver. The intensity represented the average value from five SERS spectra.

of adenine (Suh and Moskovits, 1986; Madzharova et al., 2016). The absorption time was also studied (Fig. S14), showing that the absorption get saturated after about 45 min incubation.

A "W" shape fluctuation of the Raman intensity versus the stop band of 3D-islands was observed (dashed squares in Fig. 3a and c), indicating that greater Raman enhancements could be achieved by the stop band edges overlapped with the excitation wavelength when compared with the stop band center overlapped with the excitation wavelength (Fig. 3b and d). The phenomenon was considered as a result of the enhanced light-matter interaction by the slow photon effects. As the slow photon effects were caused by the slowed group velocity at the edge of the stop band (Qi et al., 2014; Mu et al., 2015), the 3D-islands samples whose stop band edges overlapped with the excitation wavelength showed higher Raman intensity than that of the neighbouring samples. On the other hand, when the stop bands of the 3D-islands samples were far from the excitation wavelength, 3D-islands with stop bands at 431 nm exhibited higher Raman intensity than that of the neighbouring samples, which could be explained by the increased surface area and scattering ability based on the increased number of silver nanoparticles, because the sizes of Ag-islands were averagely proportional to the sizes of SiO_2 spheres (Fig. S11). Thus, the 3DPCs affected Raman enhancement by two ways: firstly by slow photon effects, secondly by Ag-islands morphology control via the SiO_2 sphere diameters.

3.3. Plasmonic-photonic crystals synergistic effects on SERS

To further evaluate the synergistic effects by the plasmonic structures and the 3DPCs contributing to Raman enhancement, the SERS activity comparison was conducted with different typical substrates (Fig. S15 and Fig. S16), including three commercial SERS substrates. All of the samples were functionalized with adenine by immersed in 5×10^{-8} M adenine solution. As the Raman spectra shown in Fig. 4a, the dominant peak at 734 cm^{-1} was assigned to the symmetric ring breathing mode, and the 1334 cm^{-1} peak was assigned to the C–N-stretching modes (Suh and Moskovits, 1986; Madzharova et al., 2016). The 3D-islands acquired a subtle SERS spectrum with the strongest signal for both peak at 734 cm^{-1} and 1334 cm^{-1}. In comparison, 2D-islands samples (Ag-islands over two-dimensional photonic crystals) exhibits an obvious peak at 1334 cm^{-1} but no detectable signal at 734 cm^{-1}. On the contrast, other samples showed much weaker Raman signal from adenine, demonstrating the significant Raman enhancement from the Ag-islands structure. As observed from the normalized Raman spectra (Fig. 4b), the 1334 cm^{-1} peaks on 3D-shells (smooth silver film over hydrophilic three-dimensional photonic crystals) and commercial substrate Q-SERS were merely detectable, while the 734 cm^{-1} peaks on them could not be observed. For other substrates, no definite characteristic peak of adenine could be detected. Furthermore, the Raman activity was confirmed by drop-casting method using 10^{-7} M MB solution, in which 3D-islands also exhibited greater enhancements than 2D-islands, 3D-shells and 2D-shells (smooth silver film over hydrophilic two-dimensional photonic crystals) (Fig. S17), demonstrating the synergistic effects of the plasmonic-photonic crystals based on enhanced electromagnetic fields, multiple scattering and slow photon effects.

The SERS activity of the samples was supported by FDTD simulations about the $|E|^2$ distribution on the surface of 3D-islands, 2D-islands, 3D-shells and 3DPCs, using the model in Fig. S18. As shown in Fig. S19, the surface $|E|^2$ of 3D-islands and 2D-islands under 633 nm incident light were much greater than those of 3D-shells and 3DPCs, indicating the major contribution of Ag-islands to the surface electric field enhancement. Additionally, the surface $|E|^2$ of 3D-islands was indeed stronger than the 2D-islands one, indicating that the 3DPCs base could lead to further electric field enhancement by slow photon effects when compared with the 2DPCs structure.

It suggests that the combination of slow photon effect and Ag-islands morphology effect (3D-islands) could realize remarkable SERS activity, stronger than the substrates with only one of the two effect. Moreover, the single Ag-islands morphology effect (2D-islands) achieves greater Raman enhancement than the single slow photon effect (hydrophobic 3DPCs). The comparison result was also supported by the FDTD simulation in Fig. S18 and Fig. S19.

3.4. Detection limits and enhancement factors for adenine and methylene blue

The capacity for quantitative detection by 3D-islands was examined using adenine, a biological molecule for nucleic acid detection, and methylene blue, a biological dye widely used for cell and tissue staining, respectively. As demonstrated in Fig. 5a, adenine as low as 5 nM could be detected on 3D-islands. The full spectrum of 5×10^{-9} M adenine absorbed on 3D-islands was showed in Fig. S20, in which the representative peaks at 734 cm^{-1} and 1334 cm^{-1} were recognizable. A

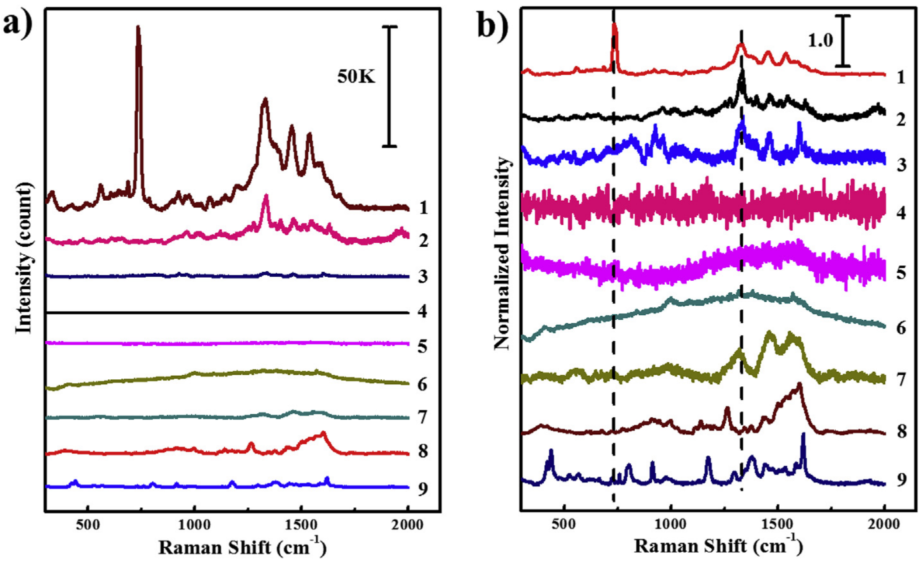

Fig. 4. (a) Raman spectra of 5×10^{-8} M adenine absorbed on various substrates and (b) the corresponding normalized Raman spectra. Spectra were measured on (1) Ag-islands over three-dimensional photonic crystals (denoted as 3D-islands), (2) Ag-islands over two-dimensional photonic crystals (denoted as 2D-islands), (3) smooth silver film over two-dimensional photonic crystals (denoted as 2D-shell, which was a typical FON substrate), (4) smooth silver film over hydrophilic three-dimensional photonic crystals (denoted as 3D-shells), (5) hydrophobic 3DPCs, (6) Ag film over quartz (denoted as Ag-films), and commercial SERS substrates of (7) Q-SERS (rough Au nanoparticles with nanogaps as shown in Fig. S16a) and (8) RAM-SERS-Au (filter paper decorated with Au nanoparticles as shown in Fig. S16b) and (9) RAM-SERS-Ag (filter paper decorated with Ag nanoparticles as shown in Fig. S16c), respectively. All the monodispersed silica nanospheres applied for 2D-islands and 3D-shells are the same as those for 3D-islands, with diameter of 264 nm. The silver deposition amount was 29 μg/cm^2. All these substrates were adsorbed with adenine in 5×10^{-8} M solutions, followed by Raman measurements.

near-linear correlation between the intensity of adenine representative peak at 734 cm^{-1} and the logarithmic concentrations was shown in Fig. 5b. The strong enhancement of 3D-island was further confirmed by drop-casting method with MB solutions. A detection limit of 10 nM for MB was achieved (Fig. 5c) as the representative peaks at 1397 and 1625 cm^{-1} were observable. Analogously, a near-linear quantitative correlation manifested by Raman intensity at 1625 cm^{-1} versus the logarithmic concentrations (Fig. 5d).

The enhancement factor (EF) for adsorption method was defined by the following equation (Le Ru et al., 2007; Oh and Jeong, 2012):

$$EF = \left(\frac{I_{\text{SERS}}}{N_{\text{SERS}}}\right) / \left(\frac{I_{\text{bulk}}}{N_{\text{bulk}}}\right) \quad (1)$$

Detailed calculation was showed in the supplementary material. Accordingly, the enhancement factor of 3D-islands, 2D-islands and 2D-shells for adenine were calculated to be 1.13×10^7, 2.95×10^5 and 1.92×10^4. Thus, compared with the traditional FON structure of 2D-shells, the EF of 3D-islands was three orders of magnitude higher.

The EFs for drop-casting method were also calculated, as the EFs for 3D-islands, 2D-islands and 2D-shells were 2.85×10^5, 1.06×10^4 and 7.40×10^3 respectively. The EF of 3D-islands was also greater than those of 2D-islands and 2D-shells.

Compared with the detection limits in recent publications as listed in Table S1 and Table S2, 3D-islands were one of the most sensitive SERS substrate for adenine and MB detection without any etching process and typical hot-spots.

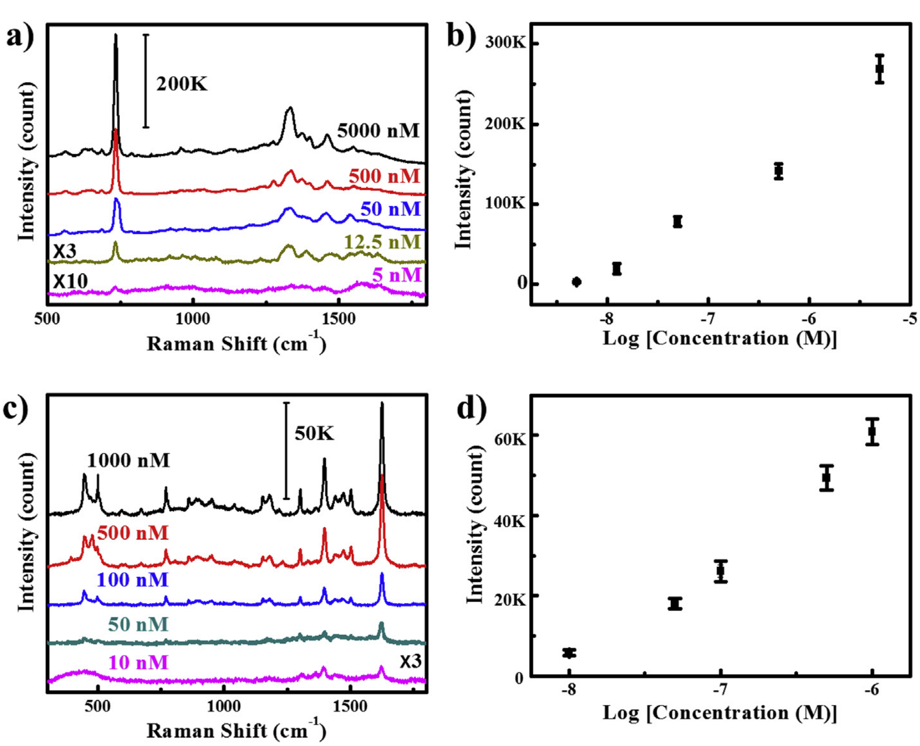

Fig. 5. (a) Raman spectra of 3D-islands absorbed with adenine by aqueous solutions of different concentrations. (b) Plot of the Raman peak intensity at 734 cm^{-1} versus the logarithmic concentrations of adenine. (c) Raman spectra of the 3D-islands substrates applied with MB aqueous solutions of different concentrations. (d) Plot of the Raman peak intensity at 1625 cm^{-1} versus the logarithmic concentrations of MB. The monodispersed silica nanospheres applied for 3D-islands were with diameter of 264 nm (stop band at 588 nm). The silver deposition amount was 29 μg/cm^2. The intensity represented the average value from five SERS spectra.

3.5. Uniformity, durability and reproducibility of 3D-islands

Uniformity, durability and reproducibility were studied to investigate the reliability and long term SERS behavior of the 3D-islands substrate. As showed in Fig. S21, the majority of Raman mapping area (80 μm × 80 μm) showed normalized intensity over 0.9, and over 98% of the area showed normalized intensity over 0.7, except serval defect spots (corresponding to the defects of 3DPC) whose normalized intensity was still over 0.5. Accordingly, it indicated decent uniformity of the enhancement by the hybrid substrates. Durability tests were carried out by monitoring Raman intensity at 1625 cm^{-1}. As shown in Fig. S22, the Raman intensity fell by half after the first ten-day storage, probably ascribed to the oxidation of the Ag nanoparticles. Afterwards, the Raman intensity kept stable over a month of storage, demonstrating the feasibility for long term activity. To investigate the reproducibility of 3D-islands SERS substrate, eight independent hybrid subsrates were fabricated. The Raman intensity of adenine 734 cm^{-1} peak was collected, and the relative standard deviation (RSD) was calculated to be 15.95%, demonstrating the acceptable reproducibility of 3D-islands (Fig. S23). More details were showed in the supplementary material.

3.6. Adenine detection in simulated urine and blood by 3D-islands

The concentration of adenine in urine and blood can be significant indicators of health (Niu et al., 2012; Yuan et al., 2019). To examine the anti-interference ability and specificity of 3D-islands substrate, and study the substrate's potential for actual sensoring, the adenine in simulated urine and blood were detected by 3D-islands. More details were showed in the supplementary material. In the simulated urine (Figs. S24a and b), even with the common interference such as urea, creatinine and uric acid, the adenine could be detected at concentration as low as 0.25 mg/L, the level of adenine concentration in actual urine sample (Yuan et al., 2019). Beside the representative peak of adenine at 734 cm^{-1}, the peak at 688 cm^{-1} was ascribed to uric acid and the peak at 1001 cm^{-1} was ascribed to urea (Huang et al., 2014). It showed a near-linear correlation between the Raman intensity at 734 cm^{-1} and the adenine concentrations, in the range from 0.25 mg/L to 4 mg/L. While in the simulated blood (Figs. S24c and d), the representive peaks of adenine at 734 cm^{-1} was still clearly detectable at 1.7 mg/L, one magnitude lower than that in actual sample (Kreuger and Åkerblom, 1980), in spite of the interference of protein (bovine serum albumin), uric acid, hypoxanthine and xanthine and the like. Similarly, the intensity of 734 cm^{-1} peak showed nearly linear correlation with the concentrations of adenine, in the range from 1.7 mg/L to 27.2 mg/L. The 3D-islands substrate manifested competitive specificity in the presence of common interference in biosensing, as well as the potential for actual detection.

3.7. Construction of 3D-islands microchip

The etching-free process of the 3D-islands enabled not only scalable preparation, but also facile and rapid fabrication for SERS microchips by direct assembly of 3DPCs. Microchips of the 3D-islands (Fig. 6a and Fig. S25) were constructed on a superhydrophobic (SHP) substrate based on raspberry-like PS@SiO_2 particles (Fig. 6b) (Ming et al., 2005; Deng et al., 2011). The fabrication details were showed in the supplementary material. The contact angle of the SHP substrate (~150°) was obviously higher than other hydrophobic substrates in this work (Fig. S26). Water droplets could hardly adhere to the SHP substrate, even after several times of contact and pressing (Fig. S27). The low adhesion was attributed to the morphological roughness of the raspberry-like particles, which could lead to dewetting during the drop-casting process. The low adhesion and high contact angle were beneficial to the enrichment of analyte (Fig. 6c).

As the solvent evaporated, the MB solution dewetted from the SHP substrate with low adhesion and finally enriched on the 3D-islands microchip, leading to higher MB density and further enhanced Raman intensity. As shown in Fig. 6d, the detection limit of MB was decreased from 10 nM from the bulk 3D-islands to 1 nM. Additionally, in the low concentration range (1 nM–50 nM), a near linear relation was observed for the intensity of MB representative peak at 1625 cm^{-1} against the logarithmic concentrations (Fig. 6e).

4. Conclusion

In conclusion, large-scale hybrid substrates of island-like Ag nanoparticles over three-dimensional photonic crystals were fabricated through an etching-free process. The optical property and SERS activity of the hybrid substrates could be tuned by the size of silver nano-islands and the photonic stop band of 3DPCs. Dramatic Raman enhancement was observed as a result of the synergy of 3DPCs (by slow photon effects) and Ag-islands (by the enhanced local electric field and scattering), which was supported by the FDTD stimulation. Adenine and MB could be detected at nM level by adsorption method and drop-casting method respectively, with good uniformity and durability. The enhancement factor was three orders of magnitude higher than the conventional film over nanosphere (FON) control group. Microchips based on the hybrid substrates were proved to be more sensitive becaused of the concentration effect. This work demonstrates the tunable optical properties and great Raman enhancement in virtue of the 3D photonic stop bands and enhanced scaterring in the hybrid structure without the help of nanogaps, paving the way for their further application in field of biological detection, medical diagnosis and the like. However, there is a major limitation in this work to be further researched, which is the lack of biosensing test in actual samples because of the limited time and condition. In future work, the detection in the actual sample should be carried out, and techniques like antibody modification should be applied, therefore the performance of the microchip in actual samples could be more selective and sensitive.

Declaration of competing interest

The authors declare that they have no known competing financial interests or personal relationships that could have appeared to influence the work reported in this paper.

The authors declare the following financial interests/personal relationships which may be considered as potential competing interests:

CRediT authorship contribution statement

Guojian Chen: Data curation, Investigation, Writing - original draft. **Kelian Zhang:** Data curation. **Baibin Luo:** Data curation. **Wei Hong:** Conceptualization, Formal analysis, Project administration, Writing - review & editing. **Jian Chen:** Resources, Writing - review & editing. **Xudong Chen:** Supervision, Funding acquisition, Writing - review & editing.

Acknowledgements

This work was supported by the National Natural Science Foundation of China (Grant No. 51833011), the Fundamental Research Funds for the Central Universities (Project No. 18lgpy36) and the Guangdong YangFan Innovative & Entrepreneurial Research Team Program (Project No. 201633002).

Appendix A. Supplementary data

Supplementary data to this article can be found online at https://doi.org/10.1016/j.bios.2019.111596.

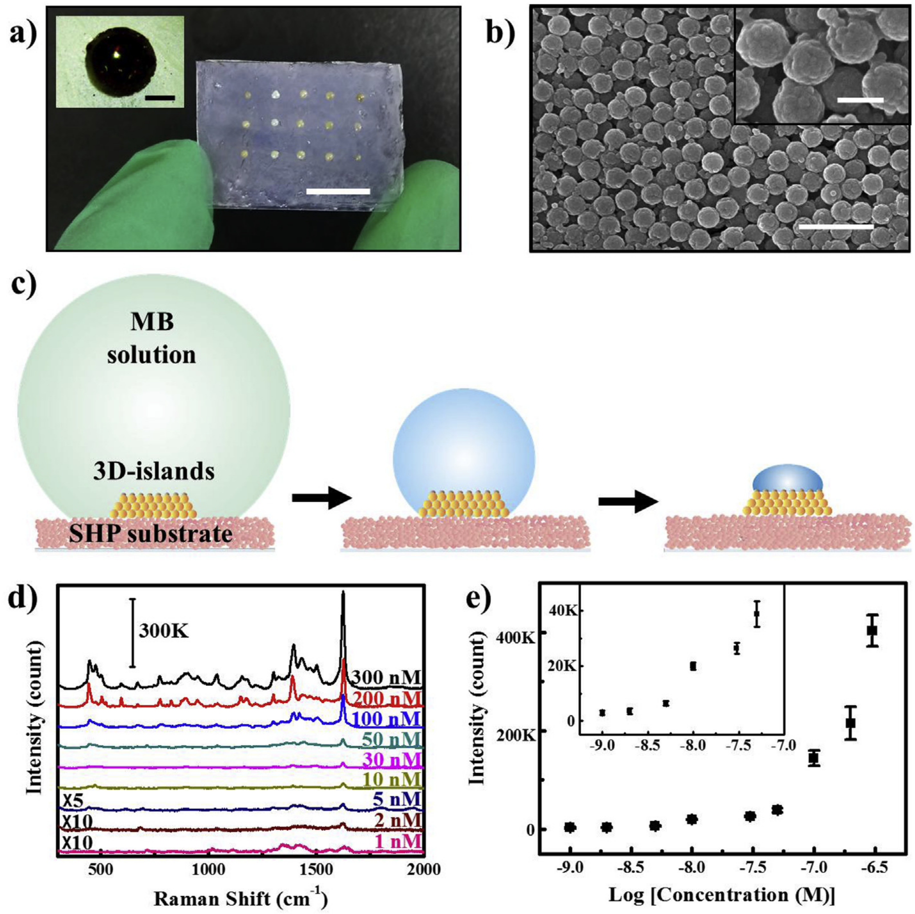

Fig. 6. (a) An optical image of 3D-islands microchips on the superhydrophobic substrate. The diameters of SiO_2 spheres forming the 3DPCs were 198 nm, 224 nm, 249 nm, 264 nm and 304 nm from left to right (with stop bands at 433 nm, 480 nm, 548 nm, 588 nm and 675 nm respectively). Scale bar: 1 cm. Inset: a microscopic image of a 3D-islands dot on a microchip, scale bar: 0.5 mm. (b) SEM image of raspberry-like PS@SiO_2 particles of the superhydrophobic substrate. Scale bar: 1 μm and 250 nm (inset), respectively. (c) Schematic showing the evaporation-concentration process of MB solution droplet on the microchip. The superhydrophobic substrate was denoted as SHP substrate. (d) Raman spectra of MB on the microchips functionaled with the aqueous solutions in different concentrations, excited by 633 nm laser. The monodispersed silica nanospheres applied for 3D-islands microchips were with diameter of 264 nm (stop band at 588 nm). The silver deposition amount was 29 μg/cm^2. (e) Plot of the Raman peak intensity at 1625 cm^{-1} versus the logarithmic concentrations of MB (from 300 nM to 1 nM). Inset: Plot of the Raman peak intensity at 1625 cm^{-1} versus the logarithmic concentrations of MB (from 50 nM to 1 nM). The intensity represents the average value from five SERS spectra. Exposure time of Raman measurement was 30 s and the spectra were accumulated for 5 times.

References

Baia, L., Baia, M., Popp, J., Astilean, S., 2006. J. Phys. Chem. B 110 (47), 23982–23986.
Banholzer, M.J., Millstone, J.E., Qin, L., Mirkin, C.A., 2008. Chem. Soc. Rev. 37 (5), 885–897.
Campion, A., Kambhampati, P., 1998. Chem. Soc. Rev. 27 (4), 241–250.
Chen, G., Wang, D., Hong, W., Sun, L., Zhu, Y., Chen, X., 2017. Small 13 (9), 1602612.
Chen, Y., Zhang, Y., Pan, F., Liu, J., Wang, K., Zhang, C., Cheng, S., Lu, L., Zhang, W., Zhang, Z., Zhi, X., Zhang, Q., Alfranca, G., Fuente, J.M., Chen, D., Cui, D., 2016. ACS Nano 10 (9), 8169–8179.
Deng, X., Mammen, L., Zhao, Y., Lellig, P., Müllen, K., Li, C., Butt, H.J., Vollmer, D., 2011. Adv. Mater. 23 (26), 2962–2965.
Ding, S.Y., Yi, J., Li, J., Ren, F.B., Wu, D.Y., Panneerselvam, R., Tian, Z.Q., 2016. Nat. Rev. Mater. 1 (6), 16021–16036.
Fang, Y., Seong, N.H., Dlott, D.D., 2008. Science 321 (5887), 388–392.
Flores-Romero, E., Rodríguez-Sevilla, E., Cheang-Wong, J.C., 2018. Photonics Nanostruct. 28, 81–87.
Gong, T., Cui, Y., Goh, D., Voon, K.K., Shum, P.P., Humbert, G., Auguste, J.L., Dinh, X.Q., Yong, K.T., Olivo, M., 2015. Biosens. Bioelectron. 64, 227–233.
Gong, Z., Du, H., Cheng, F., Wang, C., Wang, C., Fan, M., 2014. ACS Appl. Mater. Interfaces 6 (24), 21931–21937.
Gruenke, N.L., Cardinal, M.F., Mcanally, M.O., Frontiera, R.R., Schatz, G.C., Van Duyne, R.P., 2016. Chem. Soc. Rev. 45 (8), 2263–2290.
Guo, X., Guo, Z., Jin, Y., Liu, Z., Zhang, W., Huang, D., 2012. Microchim. Acta 178 (1–2), 229–236.
Hong, W., Zhang, Y., Gan, L., Chen, X., Zhang, M., 2015. J. Mater. Chem. C 3 (24), 6185–6191.
Huang, S., Wang, L., Chen, W., Feng, S., Lin, J., Huang, Z., Chen, G., Li, B., Chen, R., 2014. Laser Phys. Lett. 11 (11), 115604–115609.
Im, H., Bantz, K.C., Lee, S.H., Johnson, T.W., Haynes, C.L., Oh, S.H., 2013. Adv. Mater. 25 (19), 2677–2685.
Kang, M.S., Nazarkin, A., Brenn, A., Russell, P.S.J., 2009. Nat. Phys. 5 (4), 276–280.
Kneipp, K., Moskovits, M., Kneipp, H., 2006. Surface-Enhanced Raman Scattering. Springer, Berlin, Heidelberg, Germany.
Kreuger, A., Åkerblom, O., 1980. Vox Sanguinis 38 (3), 156–160.
Le Ru, E.C., Blackie, E., Meyer, M., Etchegoin, P.G., 2007. J. Phys. Chem. C 111 (37), 13794–13803.
Li, X., Chen, G., Yang, L., Jin, Z., Liu, J., 2010. Adv. Funct. Mater. 20 (17), 2815–2824.
Liu, Z., Wang, Y., Deng, R., Yang, L., Yu, S., Xu, S., Xu, W., 2016. ACS Appl. Mater. Interfaces 8 (22), 14160–14168.
Lin, T.L., Lin, J.H., Guo, J.T., Kan, H.C., 2015. Adv. Opt. Mater. 3 (10), 1470–1475.
Madzharova, F., Heiner, Z., Gühlke, M., Kneipp, J., 2016. J. Phys. Chem. C 120 (28), 15415–15423.
Ming, W., Wu, D., Benthem, R.V., With, G.D., 2005. Nano Lett. 5 (11), 2298–2301.
Mu, Z., Zhao, X., Huang, Y., Lu, M., Gu, Z., 2015. Small 11 (45), 6036–6043.
Nam, J.M., Oh, J.W., Lee, H., Suh, Y.D., 2016. Acc. Chem. Res. 49 (12), 2746–2755.
Nie, S., Emory, S.R., 1997. Science 275 (5303), 1102–1106.
Niu, X., Yang, W., Ren, J., Guo, H., Long, S., Chen, J., Gao, J., 2012. Electrochim. Acta 80, 346–353.
Oh, Y., Jeong, K., 2012. Adv. Mater. 24 (17), 2234–2237.
Prodan, E., Radloff, C., Halas, N.J., Nordlander, P., 2003. Science 302 (5644), 419–422.
Qi, D., Lu, L., Wang, L., Zhang, J., 2014. J. Am. Chem. Soc. 136 (28), 9886–9889.
Schatz, G.C., Young, M.A., Duyne, R.P.V., 2006. Electromagnetic Mechanism of SERS. Springer, Berlin, Heidelberg, Germany.
Schlücker, S., 2014. Angew. Chem. Int. Ed. 53 (19), 4756–4795.
Sharma, B., Frontiera, R.R., Henry, A.I., Ringe, E., Van Duyne, R.P., 2012. Mater. Today 15 (1–2), 16–25.
Stöber, W., Fink, A., Bohn, E., 1968. J. Colloid Interface Sci. 26 (1), 62–69.
Suh, J.S., Moskovits, M., 1986. J. Am. Chem. Soc. 108 (16), 4711–4718.
Sun, L., Hong, W., Liu, J., Yang, M., Lin, W., Chen, G., Yu, D., Chen, X., 2017. ACS Appl. Mater. Interfaces 9 (51), 44503–44511.
Sun, L., Yang, M., Huang, J., Yu, D., Hong, W., Chen, X., 2016. Adv. Funct. Mater. 26 (27), 4943–4950.
Wang, D., Zhu, W., Best, M.D., Camden, J.P., Crozier, K.B., 2013. Nano Lett. 13 (5), 2194–2198.
Xiao, G.N., Man, S.Q., 2007. Chem. Phys. Lett. 447 (4–6), 305–309.
Yang, T., Guo, X., Wang, H., Fu, S., Yu, J., Wen, Y., Yang, H., 2014. Small 10 (7), 1325–1331.
Yuan, Y., Jiang, M., Zhang, H., Liu, J., Zhang, M., Hu, P., 2019. J. Sep. Sci. https://doi.org/10.1002/jssc.201900170.
Zhang, X., Xiao, X., Dai, Z., Wu, W., Zhang, X., Fu, L., Jiang, C., 2017. Nanoscale 9 (9), 3114.
Zhang, X., Young, M.A., Lyandres, O., Duyne, R.P.V., 2005. J. Am. Chem. Soc. 127 (12), 4484–4489.
Zhao, H., Jin, J., Tian, W., Li, R., Yu, Z., Song, W., Cong, Q., Zhao, B., Ozaki, Y., 2015a. J. Mater. Chem. 3 (8), 4330–4337.
Zhao, X., Xue, J., Mu, Z., Huang, Y., Lu, M., Gu, Z., 2015b. Biosens. Bioelectron. 72, 268–274.
Zhu, W., Esteban, R., Borisov, A.G., Baumberg, J.J., Nordlander, P., Lezec, H.J., Aizpurua, J., Crozier, K.B., 2016. Nat. Commun. 7, 11495.